Development and Validation of a Novel M6A-related LncRNA Prognostic Signature Associated with Immune Microenvironment for Ovarian Serous Cystadenocarcinoma

Rui Geng
Nanjing Medical University
Tian Chen
The First Affiliated Hospital of Nanjing Medical University
Zihang Zhong
Nanjing Medical University
Senmiao Ni
Nanjing Medical University
Jianling Bai (baijianling@njmu.edu.cn)
Nanjing Medical University
Jinhui Liu
The First Affiliated Hospital of Nanjing Medical University

Research Article

Keywords: Ovarian Serous Cystadenocarcinoma, N6-methyladenosine, long non-coding RNAs, prognosis, tumor microenvironment

Posted Date: December 2nd, 2021

DOI: https://doi.org/10.21203/rs.3.rs-1120501/v1

Abstract

Background: OV is the most lethal gynecological malignancy. M6A and lncRNAs have great influence on OV development and patients' immunotherapy response. Here, we decided to establish a reliable signature in the light of mRLs.

Method: The lncRNAs associated with m6A in OV were analyzed and obtained by co-expression analysis in the light of TCGA-OV database. Univariate, LASSO and multivariate Cox regression analyses were employed to establish the model in the light of the mRLs. K-M analysis, PCA, GSEA, and nomogram based on the TCGA-OV and GEO database were conducted to prove the predictive value and independence of the model. The underlying relationship between the model and TME and cancer stemness properties were further investigated through immune features comparison, consensus clustering analysis, and Pan-cancer analysis.

Results: A prognostic signature comprising four mRLs: WAC-AS1, LINC00997, DNM3OS, and FOXN3-AS1, was constructed and verified for OV according to TCGA and GEO database. The expressions of the four mRLs were confirmed by qRT-PCR in clinical samples. Applying this signature, people can identify patients more effectively. All the sample were assigned into two clusters, and the clusters had different overall survival, clinical features, and tumor microenvironment. Finally, Pan-cancer analysis further demonstrated the four mRLs significantly related to immune infiltration, TME and cancer stemness properties in various cancer types.

Conclusion: This study provided an accurate prognostic signature for patients with OV and elucidated the potential mechanism of the mRLs in immune modulation and treatment response, giving new insights into identifying new therapeutic targets.

Introduction

Ovarian cancer a gynecological malignancies, especially for women aged 40 to 79(1). And OV a common type of this cancer, the proportion of OV is ninety percent in all patients with ovarian cancer (2). On account of lacking specific initial symptoms and sensitive biomarkers for early diagnosis, most OV patients cannot be diagnosed at an early stage and the progression always rapid(3, 4). Consequently, developing novel and reliable signatures to diagnoses and prognoses OV in early stage is an urgent need.

The results of randomized trials show that transvaginal ultrasound and CA-125 testing are of little help to diagnoses ovarian cancer and changing the mortality rate(5).

Therefore, more attention has been paid to discovering key regulatory genes involved in cancer pathogenesis and progression and constructing prognostic signatures based on them. Recently, as a reversible epigenetic modification of various RNAs, the vital role and molecular mechanisms of m6A RNA modification in cancer pathogenesis, drug response, and developing new targets for therapy have been intensely studied and confirmed(6). What’s more, it has also been found that m6A RNA modification

functions in immunity, which provides insights into cancer immunotherapy(7). M6A is dynamically regulated by three types of proteases with distinct functions, namely “writers, “erasers”, or “readers”(8, 9). Changing the structure of RNA can influence a variety of cell processes. As the result, the effect of mRLs may play important roles for the transfer of cancer cells.

LncRNA is a group of RNA molecules. Although lncRNA cannot be translated into protein, it has a vital effect on many biological processes like the tumorigenesis and development (10-12). The relationship between m6A and lncRNAs is under in-depth study. Extensive studies have revealed that the biogenesis and functions of lncRNAs depend on m6A modification(13-15). YTHDF1 and YTHDF2, m6A readers, modify the stability of oncogenic lncRNA THOR thus promoting the biological behavior of cancer cells (16). LncRNA RP11 dependent on m6A induction can trigger colorectal cancer metastasis by preventing the degradation of Zeb1(17). In addition, m6A modification is also adversely affected by lncRNAs (18), and they can function together to regulate protein translation(18, 19). For instance, LINRIS stabilize IGF2BP2 (an m6A reader) by preventing its K139 ubiquitination, thus promoting colorectal cancer cell line growth (20). In OV, the stability of RHPN1-AS1 is improved by m6A modification, promoting the proliferation and metastasis of OV cell(21). Hence, linking m6A and lncRNA, and further studying the function and molecular mechanism of mRLs in tumorigenesis and progression can affect the overall survival rate of OV. However, such research on OV is still lacking.

This study established and verified a mRLs prognostic signature for OV in the light of TCGA and GEO database. The underlying correlation between the signature and TME, as well as therapeutic response, was also explored. Besides, clustering subgroups and pan-cancer analysis were also used to verify the application value of the model in distinguishing patients in terms of prognosis and therapeutic response.

Materials And Methods

2.1 Collecting and disposing data

The flow chart of our study is performed in **Figure 1A**. We collected gene expression profiling and clinicopathological data of OV samples from TCGA dataset (https://cancergenome.nih.gov/) and the GSE9891 database (http://www.ncbi.nlm.nih.gov/geo/). The single gene expression in OV samples with different stages was obtained from GEPIA (http://gepia.cancer-pku.cn/index.html)(22). For the purpose of identifying the role of the four mRLs in more cancers, we also got the pan-cancer data of 33 cancers from UCSC Xena database (https://xenabrowser.net/datapages/)(23), including RNA-seq, immune subtypes, prognosis profiles, stemness scores.

2.2 Identification of mRLs associated with OV prognosis

Firstly, the expression matrix of 23 m6A regulators(METTL3, METTL14, METTL16, WTAP, VIRMA, ZC3H13, RBM15, RBM15B, YTHDC1, YTHDC2, YTHDF1, YTHDF2, YTHDF3, HNRNPC, FMR1, LRPPRC, HNRNPA2B1, IGFBP1, IGFBP2, IGFBP3, RBMX, FTO and ALKBH5) was achieved from previous studies (24). Secondly, Pearson correlation analysis was implemented to select 419 mRLs according to

the standard of $p < 0.05$ and absolute correlation coefficient > 0.3, then 61 mRLs shared in both TCGA and GEO were obtained after the removal of batch effects through combat via the “sva” R package. Finally, we collected 374 samples with sufficient prognostic clinical data and lncRNAs expression information from TCGA. The 374 samples from the TCGA-OV dataset were assigned into TCGA-train (n=187) and TCGA-test (n=187) according to 1:1 randomly, and we employed train set to build the signature. The test set (187 samples), the entire set (374 samples), and the GSE9891 database (278 samples) were applied for validation and further research. Univariate Cox regression analysis was applied to screen the relationships between mRLs related to patients’ prognoses in the TCGA-train set by the survival package of R (http:// bioconduct or. org/ packages/ survivalr/).

2.3 RNA isolation and qRT-PCR

The research was approval by the First Affiliated Hospital of Nanjing Medical University ethics committee, and the peoples took part in the study all signed the informed consent. Total RNA of the OV and normal tissues was obtained through TRIzol reagent (Thermo Fisher Scientific, Waltham, MA, USA), whose integrity was estimated by the Agilent Bioanalyzer 2100 (Agilent Technologies, Santa Clara, CA, USA). cDNA synthesis was conducted by the high-capacity reverse transcription kits (TaKaRa, Shiga, Japan) and then qRT-PCR was based on SYBR Green PCR Kit (Thermo Fisher Scientific) and the $2^{-\Delta\Delta Ct}$ method on Light Cycler 480 (Roche, Switzerland). GAPDH was the endogenous control. Primer sequences for GAPDH and four mRLs were presented in **Table S3**.

2.4 Establish and proof of an mRL prognostic signature for OV

The model was established by using LASSO in TCGA-train. Then the multivariate regression analysis was conducted determine mRLs with predict independence. The format to assess the risk score was: . The patients were divided into two groups in terms of median risk score of train set. Kaplan-Meier analysis was conducted through the “survival” R package to against the OS of the groups. Through the “ROC” R package, the ROC were depicted and the AUC were calculated to ESTIMATE its specificity and sensitivity. PCA was used to prove the grouping ability of the model by grouping visualization of high-dimensional data of risk model(25). We also conducted subgroup analysis to verify the prognostic ability of the mRL model. Univariate and multivariate Cox analysis were applied to assess whether the signature was an independent factor.

2.5 Establishment and validation of a nomogram

For the purpose of improving the predictive ability of the mRL signature, we established a nomogram compromised of the signature, patient age, grade, and tumor stage. Calibration curves were applied to explore the accuracy and reliability of the nomogram.

2.6 Gene set enrichment analysis

As our previous study(26), we performed function annotation through GSEA to reveal potential mechanisms in different risk groups. KEGG in GSEA was applied to select predefined gene sets; 5000 permutations were conducted in terms of the gene set to calculate p-values. GSEA was analyzed using “clusterProfiler” package(27).

2.7 The Correlation between the signature and tumour infiltration immune cells (TIICs)

CIBERSORT was employed to assess the abundance of TIICs profile in all tumor tissues. We assessed the proportion of 22 types of TIICs in every patient according to the CIBERSORT score(28). Furthermore, the correlation between the lncRNAs and TIICs score was evaluated to identify which immune cells had distinguish between cancers.

2.8 The correlation to other immune features

ESTIMATE was used to compute the proportion of immune and stromal components in TME for each sample(29). The relationships between lncRNA expression and the risk score were calculated by Spearman correlation. Furthermore, we identified six immune types and used the analysis of variance (ANOVA) to evaluate the relationships between these subtypes and lncRNAs expression. Cancer stem cell-like properties data were employed to assess stemness characteristics of cancer cells. The association between stemness features and lncRNA was also evaluated by Spearman analysis.

2.9 Immunotherapy response prediction

Immunophenoscores (IPSs) are calculated based on four major categories of genes expression z-scores to evaluate and compare the potential reaction to ICI between the two groups, and the high scores represent high immunogenicity(30). IPSs data of each OV patient in TCGA-entire were achieved from The Cancer Immunome Atlas (TCIA) (https://tcia.at/home).

2.10 Assess drug sensitivity

The newest CellMiner version (https://discover.nci.nih.gov/cellminer/) could help researchers achieve the NCI-60 data flexibly for correlations between genomic, molecular, and pharmacologic parameters(31). We collected the expression of 4 m6A-related genes and z-score for cell sensitivity data (GI50) from the webpage and used Pearson correlation coefficient to assess the influence of the m6A-related gene expression on drug sensitivity.

2.11 Consensus clustering

The expression of the lncRNAs was utilized to recognize the subtypes in OV patients via “ConsensusClusterPlus” R package (http://www.bioconductor.org/). We used the log-rank test and K–M curve to calculate the OS difference between groups.

2.12 Statistical analysis

R 4.0.2 was used to do statistical analyses. The relationships of risk score or mRLs expression level to stemness score, estimate score and drug sensitivity was calculated by Spearman or Pearson correlation analysis. Univariate or multivariate regression analyses were applied to calculate the relationships between the four mRLs with patients' OS. Kaplan-Meier analysis could compare the survival state between the groups. Time-dependent ROC curve analysis could test the predict ability of the model. Subgroup analysis could evaluate the stability of the prognostic signature in subgroups stratified by clinical characteristics. Student's t-test and ANOVA were applied to find the distinguish between different groups. Linear mixed-effect models were used for pan-cancer analysis. The hazard ratio and 95% confidence interval were assessed to screen prognosis-related genes. $P < 0.05$ was regarded has statistical significance.

Results

3.1 Identification of mRLs in OV

Firstly, we abstracted the expression of lncRNAs from TCGA-OV dataset and identified 419 mRLs ($p < 0.05$, absolute correlation coefficient > 0.3) through Pearson correlation analysis with m6A regulators. The relational network between m6A regulators and mRLs was shown in **Figure 1B**. After collecting the expression of lncRNAs in the GSE9891 dataset, we found 61 mRLs shared in both datasets. When combined with clinical information, we screened five mRLs related to prognosis through univariate regression analysis in TCGA-train (**Table S2**).

3.2 Establish and verify of a prognostic signature based on mRLs in OV patients

Firstly, the 374 OV patients in were classified into train and test sets at a 1:1 ratio randomly, including 187 OV patients, respectively. Secondly, we performed the LASSO (**Figure S1A-B**) and multivariate regression analysis (**Figure S1C**) in train set to build a reliable prognostic signature. The formula was as following:

Risk core= (-0.068088177 * expr (WAC-AS1)) + (-0.276777737 * expr (LINC00997)) + (0.09155959 * expr (DNM3OS)) + (-0.137781856 * (FOXN3-AS1), expr means the expression value. WAC-AS1, LINC00997, DNM3OS, and FOXN3-AS1 were finally identified as key mRLs. Both the outcomes of the expression analyses in the GEPIA dataset and the qRT-PCR results indicated that the expression of DNM3OS and FOXN3-AS1 were higher in normal compared with tumor tissue ($p <0.05$) (**Figure S2A-H**). Afterward, we assessed the risk score of OV patients in TCGA-train and separated them into two groups. The distributions of risk score, survival status of each sample (**Figure 2A**), and the heatmap of key gene expression patterns (**Figure 2E**) in TCGA-train were performed in **Figure 2**. People in high risk had poor survival prognosis than low-risk groups in TCGA-train (**Figure 2I**). Time-dependent receiver operating characteristic curves (ROC)analysis based on the signature revealed that the AUC of 1-, 2-, and 3-years survival was 0.624, 0.694, and 0.630, respectively (**Figure 2M**). To verify the mRL prognostic signature, we calculated the risk score of the patients in TCGA-test (N=187), TCGA-entire (N=374), and GEO datasets (N=278) and divided patients into either group in terms of the median risk score of the TCGA-train (**Figure 2B-D**). The heatmap all showed that except for DNM3OS, the expression of WAC-AS1, LINC00997, and

FOXN3-AS1 was higher in low-risk groups (**Figure 2E-H**). The Kaplan-Meier analyses of the TCGA-test, TCGA-entire, and GEO datasets revealed the same trend that the OV patients with low risk had higher OS than high-risk group ($p < 0.01$) (**Figure 2J-L**). Furthermore, time-dependent ROC curve indicated the predict capability of the prognostic signature based on mRLs. The AUC of 1-, 2- and 3-years survival in three sets were shown in **Figure 2N-2P**. In addition, the distributions of the groups were different in PCA plots (**Figure S3**). These results all demonstrated the accurate and reliability of the mRL prognostic signature in OV prediction.

3.3 The relationships between the model and clinical factors

The correlations between risk core and clinical characteristics are performed in **Figure S4A-F**. The risk score in age≤60 group was lower than group which age > 60 ($p < 0.05$, **Figure S4D**), and the proportion of older patients with high-risk score is 52%, while that people with low-risk score was 40% (**Figure S4A**). But the difference of risk score in the groups assigned by tumor grade and tumor stage was not significant (**Figure S4B-C, E-F**). What's more, the risk score of high-immune score group was markedly higher than lower score patients ($p < 0.05$, **Figure S4G**), and the significant difference could be found in the risk core of Cluster1 and Cluster2 subgroups ($p < 0.05$, **Figure S4H**). Stratification analysis grouped by patient age, tumor grade, and tumor stage performed that the OS of patients with high risk was worse than that low-risk group (**Figure S4I-N**). By comparing the patients' state between the groups, we also found a higher mortality of patients with high risk (**Figure S5A**), and the risk scores of dead patients were statistically higher than alive patients ($p =0.002$, **Figure S5B**). K–M curves of OS for patients subjected to chemotherapy performed that people with high risk had poorer prognoses than those with lower risk ($p <0.001$, **Figure S5C**). In patients with BRCA1, low-risk groups also had a favourable survival outcome (**Figure S5D**).

3.4 Clinical application of the signature

Univariate and multivariate regression analyses in TCGA-train, TCGA-test, TCGA-entire, and GEO datasets all indicated the independence of the mRL model (**Table S3**). Moreover, patient age and tumor stage were also crucial poor prognostic factors for OV. To advance the predict performance of the signature, we built a nomogram comprising the risk score, age, grade, and stage in both TCGA (**Figure 3A**) and GEO datasets (**Figure S6**). **Figure 3B-D** revealed that the predicted rates of OS were highly consistent with the observed rates. In addition, the prognostic signature showed superior predictive ability than clinical characteristics, and when combined with clinical characteristics, the model showed better predictive power than the signature used only (**Figure 3E**).

3.5 The correlations between the mRL prognostic signature and TME

GSEA indicated that pathway related to immunity were enriched in people with high-risk score (**Figure 4A-B**). Firstly, we implemented the ESTIMATE algorithm which indicated that the stromal score, immune score, and ESTIMATE score were higher in the high-risk group ($p < 0.05$), and the risk score had positive association with them (**Figure 4C-H**). The same trends were found in the GEO dataset (**Figure 4I-N**). Then

through comparison of 22 TIICs between the groups, we identified that Dendritic cells resting and Macrophages M2 were positively related to risk score and ($p < 0.05$) and the infiltration level of T cells follicular helper and T cells regulatory (Tregs) had negative correlation with risk score ($p < 0.05$) in TCGA dataset (**Figure 5A-I**). In the GEO dataset, the risk score had positive correlation with T cells gamma delta and T cells CD4 memory resting, while risk score has negative relationship with Tregs, NK cells resting, and Dendritic cells activated (**Figure S7**). The differences in immune score and abundance of TIICs between the groups showed that patients with high risk had a repressive immune phenotype, which could partly explain the poorer OS of people with high risk.

To identify the immunological role of the four mRLs, we assessed their association with the TIICs through CIBERSORT algorithm. We found DNM3OS had significantly association with T cells follicular helper, Macrophages M2 and B cells memory ($p < 0.001$); WAC-AS1 was correlated with T cells follicular helper and Macrophages M2 ($p < 0.001$) (**Figure S8A**). Besides, WAC-AS1 ($R = -0.15$, $p = 0.0041$) and LINC00997 ($R = -0.23$, $p < 0.001$) had negative relationships with immune score, whereas DNM3OS ($R = 0.13$, $p = 0.008$) and FOXNS-AS1 ($R = 0.19$, $p < 0.001$) were positively related to immune score (**Figure S8B**). Next, to clarify the potential mechanisms of the lncRNAs in tumor progression, we used GSEA analysis to find the enriched pathways of the mRLs in OV (**Figure S8C-F**). DNM3OS was highly enriched in the calcium signaling pathway, the focal adhesion pathway, the hematopoietic cell lineage pathway, the neuroactive ligand-receptor interaction pathway, and cancer pathways.

The expression level of PD-L2 was higher in tumour tissues than in normal tissues ($p < 0.05$, **Figure 6A**), and the it was markedly higher in people with high risk score in both TCGA and GEO dataset ($p < 0.05$, **Figure 6C-F**), suggesting that people in high risk promise to benefit less from immune checkpoint inhibitor (ICI). In addition, LINC00997 showed a high correlation to PD-L2 (**Figure 6B**), so the function of LINC00997 in the tumour immune microenvironment deserved further research. Comparing the IPSs between the groups, low-risk groups had significantly higher IPSs, suggesting a more immunogenic phenotype (**Figure 6G-J**). These results all demonstrated that the signature promised to predict the efficacy to immunotherapy for OV patients.

3.6 Consensus clustering for mRLs related to OV prognosis and TME

After the consensus clustering, OV patients in TCGA dataset were classified into Cluster1 and Cluster2 subgroups in the light of the expression of the significant prognostic mRLs (**Figure 7A-D**). The heatmap of the expression pattern between cluster1 and cluster2 subgroups was performed in **Figure 7E**. In addition, the stroma, immune, and ESTIMATE scores were markedly higher and the tumor purity was substantially lower ($p < 0.05$) in Cluster2 (**Figure 7G-J**). Besides, the infiltration of B cells naive ($p < 0.05$), T cell CD4 memory activated ($p < 0.05$), T cells follicular helper ($p < 0.05$), Macrophages M1 ($p < 0.05$) and Mast cells resting ($p < 0.05$) were higher in Cluster1 subgroup, whereas the abundance of Macrophages M0 ($p < 0.05$), Macrophages M2 ($p < 0.05$), Mast cells activated ($p < 0.05$) and Neutrophils ($p < 0.05$) were higher in Cluster2 subgroup (**Figure 7F**), so Cluster2 subgroup tended to behave a more immune-suppressive phenotype. Moreover, the results of Kaplan-Meier analyses performed that the OS of

the Cluster2 was dramatically worse than that of Cluster1 (**Figure 7K**), and the expression of PD-L2 was higher in the Cluster2 (**Figure 7L**); this indicates patients in the Cluster2 may respond more sensitively to immunotherapy. The above results all demonstrated that the expression of the mRLs influences the TME, leading to different prognoses.

3.7 The expression and immune status of lncRNAs in pan-cancer

We achieved the pan-cancer data of 33 cancers from TCGA to further study the relationships between the four mRLs and immune features, stem-like properties, and patients' prognoses in pan-cancer. The expression pattern of lncRNAs in 33cancers (**Figure 8A-D**) and the heatmap (**Figure S9A**) showed inter-tumor heterogeneity, but in most cancers, the expression level of WAC-AS1 was higher in tumor tissues, whereas the expression level of DNM3OS was opposite, which were consistent with the expression trend in OV (**Figure S2**). The expression distribution of the four mRLs across all 33 cancer types showed the same trend as the above results (**Figure 8E**). Moreover, there is no significant correlation between the key mRLs **(Figure S9B**). The Kaplan-Meier analyses (**Figure S9C**) and univariate regression (**Figure S10A**) analyses showed that the role of the mRLs in the survival of patients with different cancers varied.

To identify the relationships between the key mRLs and immune features in pan-cancer, we investigated the immune subtype and the landscape of correlation with stromal score, immune score, stemness scores based on DNA-methylation (DNAss)and stemness scores based on mRNA (RNAss). Through an extensive immunogenomic analysis of pan-cancer, six immune subtypes, including wound healing (C1), IFN-γ dominant (C2), inflammatory (C3), lymphocyte depleted (C4), immunologically quiet (C5), and TGF-β dominant (C6), were identified according to differences in immune, genetic and clinical features, in which C3 had great OS, C2 and C1 had poor prognosis, while C4 and C6 had the least favorable outcomes(32). We evaluated the correlations between the mRLs expression level and the six immune subtypes, and found that all of them were related to pan-cancer immune subtypes, and elevated C1, C2, and C6 subtypes with upregulated expression of DNM3OS (**Figure 9A**). Additionally, DNM3OS had positive correlation with stromal score and immune score, whereas WAC-AS1 and LINC00997 were negatively related to stromal and immune score (**Figure 9B-D**), which showed the similar correlation in OV. All the four key mRLs were negatively related to RNAss (**Figure 9E**). Therefore, the four mRLs were took part in the formation of specific TIME. Finally, we applied the CellMiner database to evaluate the correlation between the mRLs and drug sensitivity. A higher Z-score means higher sensitivity to one specific drug. Significantly, the expression of FOXNS-AS1 influenced drug sensitivity in various cell lines (**Figure S10B**).

Discussion

Owing to the rapid progression and disability of early diagnosis, people with OV face a poor OS, with five-year survival rates below 45%(33). More and more efforts have been made to discover robust and sensitive predictive models for early diagnosis and prognosis prediction, including models based on immune genes, autophagy-related genes, m6A regulators, and so on(34-38). We found emerging evidence

proving that m6A modification had a crutial effect in the formation of TME landscape heterogeneity and complexity(39-41). Zhang et al. constructed an m6A score and demonstrated that a low m6A score was correlated to high mutation burden, an inflamed TME phenotype, and improved survival(42). As the main modification for RNAs, m6A modifications almost regulate all biological pathways, and their changes in tumors reprogram the tumor immune microenvironment, helping tumor cells escape and metastasize(15, 43). This study focused on mRLs, established a signature for OV patients, and validated its predictive capability using TCGA and GEO datasets.

The model was established based on 4 mRLs associated with patients' prognoses, including DNM3OS, WAC-AS1, FOXNS-AS1, and LINC00997, among which DNM3OS was correlated with high risk, while the others were correlated with low risk score. It was proved that over expression of DNM3OS took part in the development of ovarian cancer (44). WAC-AS1, a competing endogenous RNA, have an great influence on the regulation of tumor glycolysis(45). And the prognoses of glioma patients had low WAC-AS1 expression were better than high expression group(46). Contrary to our results, it was reported that LINC00997 had positive relationship with the metastasis and development of colorectal cancer(47). Subsequently, OV patients were separated into two groups in terms of the median risk score, and the patients in higher risk had wores prognosis . Multivariate Cox regression analysis performed that the model had a great effect on OS. ROC analysis proved that the model was more accurate than single clinical characteristics to predict outcomes of OV. We constructed a nomogram for clinical application. GSEA revealed that people with high risk score was significantly enriched in immune response and immune system process pathways. We believe that the mRLs can take part in the mechanisms of tumorigenesis and progression of OV, and the signature might provide an accurate prediction and a theoretical foundation for the treatment of OV.

Due to the resistance to chemotherapy, patients with OV ultimately die of recurred lesions after surgical removal. To improve the prognoses of OV patients, new treatment modalities emerged, especially immunotherapy, which could boost the patients' immune system to find and kill tumor cells. The immune landscape of an OV patient determines their specific response to various treatments and subsequent prognosis. The proportion of intratumoral CD8+TILs, CD4+ Treg, macrophages, and MDSC were significantly correlated with patients' outcomes(48-50). This finding has led to several stratification strategies, such as based on the number of CD8+TILs(50), six immune subtypes(32), or cytotoxic immunophenotypes(51) to identify those who benefit from immunotherapy. After validating the mRL prognostic signature in TCGA and GEO datasets, we performed immune subtype, consensus clustering, and pan-cancer analyses to research further their function when regulate TME and the underlying molecular mechanism of interaction between lncRNA and m6A regulators in OV.

TIME is associate with cancer occurrence and progression(48, 52). This study calcuated the correlation between the signature and TME in OV. According to the above results, high immune scores means higher risk scores. Some publicted articles showed that OV higher immune scores patients had poorer prognosis(53, 54), consistent with our findings. After that, positive associations was identified between the risk score and Dendritic cell resting, Macrophages M2, T cell gamma delta as well as T cells CD4

memory resting, while negative associations were identified between the risk score and T cells follicular helper infiltration, Tregs and NK cells resting. TIICs in the TME have been sought related to the prognoses of OV patients(55). For example: tumor-infiltrating macrophages with an M2 phenotype showed immunosuppressive activity, negatively related to OS(56). It was also reported that the function of Dendritic cell resting could be inhibited through GDF-15 interacting with CD44, thus facilitating ovarian cancer immune escape(57). Therefore, the high level of Macrophages M2 is closely correlated with a higher risk score and poorer prognosis, while resting NK cells infiltration mediated improved survival in ovarian cancer(58, 59). Therefore, bad clinical prognosis of high-risk patients may be associated with TIICs, and mRLs may role as significant regulators of TIICs infiltration in OV.

Cancer cells can create an immune-suppressive microenvironment through activating immune checkpoint pathways, thus achieving immune escaption(60). Therefore, blocking the role of immune checkpoints in cancer treatment has attracted people's attention. Some ICIs have been approved for clinical application in several human malignancies(61). Although there was no study found improvement of survival in clinical trials, including using ICIs targeting PD1, PD-L1, and CTLA4 in OV(62), the development in identifying treatment targets, predicting treatment response, screening potential drugs and providing new immunotherapy, will provide new breakthrough for combined and personal therapy of OV(63). The relationships between mRLs and immune checkpoint expression indicated that the risk score had positive relationship with PD-L2 expression level. The high expression of immune checkpoint ligand PD-L2 represents a suboptimal response to ICIs(64). The low-risk groups exhibited higher IPSs, indicating they may benefit more from immunotherapy, which is consistent with previous research that the anti-tumor responses mediated by ICIs depend on basic immunophenotypes(65-68)Based on. the above results, we propose that our risk signature may help predict immunotherapy efficacy for OV. After that, our study supplies new orientations into the biological mechanism of mRLs in the occurrence and progression of OV.

After that, we conducted consensus clustering analysis to screen m6A-related genes of OV and achieved two clusters according to the expression of 4 mRLs. We found the expression of WAC-AS1, LINC00997, and FOXN3-AS1 were higher, and the expression of DNM3OS was lower in Cluster 1; thus, patients in Cluster 1 had lower risk scores. We compared biological characteristics between the two clusters to further clarify the relationships between immune features and the mRLs. Cluster 1 showed higher infiltration of B cells naive, T cells CD4 memory activated, T cells follicular helper and Macrophages M1 than Cluster 2, while Cluster 2performed higher infiltration of Macrophages M2 than Cluster 1. The estimate score were higher in Cluster 2, and the tumor purity was higher in Cluster 1, which was consistent with the above results. The Kaplan-Meier analysis suggested that Cluster 2 had poor prognosis. what's more, the expression of PD-L2 was higher in Cluster 2, which suggested that Cluster 1 would tend to respond more sensitively to ICIs. How m6A modification influences tumor microenvironment, especially the TIIC types, has been researched(42, 69, 70); our study might provide more evidence for further research.

Finally, we used pan-cancer analysis to further study the role of the mRLs in different cancers. The expression pattern of the four mRLs in pan-cancer showed inter-tumor heterogeneity, but in most cancer types, WAC-AS1 had a higher expression in tumor tissues, whereas the expression level of DNM3OS was the opposite, which were consistent with the expression trend in OV. By calculating the correlation between the lncRNAs and immune features, we found DNM3OS was closely related to Macrophages M2 ($p < 0.001$) in OV, elevated C1, C2, C6 subtypes, and immune score with upregulated expression of DNM3OS in pan-cancer. Das et al. proved that overexpression of DNM3OS promoted macrophage inflammatory phenotype, immune response genes, and phagocytosis(71). It was also reported that the function of DNM3OS was cooperated by miR-214 through the proinflammatory TLR4/IFN-γ/STAT1 pathways regulated pericystic macrophage accumulation(72). These findings all demonstrated that the mRLs are token part in establishing the TME and significantly influence OS.

Our study still has several limitations. First, the results were entirely based on open accessed databases, lacking our cohort and external multicenter cohorts for validation. Second, the interactions between mRLs and m6A regulators and the mechanism of the function of lncRNAs in TME were not demonstrated by experiments. Third, it needs to apply the prognostic signature in the real world to explore its sensitivity and efficiency in classifying patients for target therapies.

Conclusion

In conclusion, our study established an independent and reliable predict signature in the light of the mRLs, and systematically evaluated its predictive accuracy and role in TIME. Consensus clustering analysis and Pan-cancer analysis demonstrated the vital role of the specific mRLs in different cancer types, which may help discovering novel therapeutic targets for OV.

Abbreviations

ANOVA: analysis of variance

AUC: area under the curve

CI: confidence interval

DNAss: stemness scores based on DNA-methylation

GEO: Gene Expression Omnibus

GSEA: gene set enrichment analysis

HR: hazard ratio

ICIs: immune checkpoint inhibitors

IPSs: Immunophenoscores

LASSO: least absolute shrinkage and selection operator

lncRNAs: long-noncoding RNAs

m6A: N6-methyladenosine

mRLs：N6-methyladenosine related long-noncoding RNAs

OS: overall survival

OV: ovarian serous cystadenocarcinoma

PCA: Principal-component analysis

qRT-PCR: quantitative real-time PCR

RNAss: stemness scores based on mRNA

ROC: receiver operating characteristic curves

ssGSEA: Single Sample Gene Set Enrichment Analysis

TCGA: The Cancer Genome Atlas

TCIA: The Cancer Immunome Atlas

TIICs: tumor-infiltration immune cells

TME: tumor microenvironment

Treg: regulatory T cells

Declarations

7.1 Availability of data and materials

The datasets supporting the conclusions of this article are included within the article.

7.2 Authors' contributions

Jianling Bai, Jinhui Liu contributed to the conception of the study; Rui Geng contributed significantly to analysis and manuscript preparation; Tian Chen performed the data analyses and wrote the manuscript; Zihang Zhong and Senmiao Ni helped perform the analysis with constructive discussions.

7.3 Acknowledgements

We would like to thank the researchers and study participants for their contributions.

7.4 Funding

Not applicable

7.5 Competing interests

The authors declare that they have no competing interests

7.6 Consent for publication

Not applicable.

7.7 Ethics approval and consent to participate

The research was approval by the First Affiliated Hospital of Nanjing Medical University ethics committee.

References

1. Siegel RL, Miller KD, Jemal A. Cancer statistics, 2019. CA Cancer J Clin. 2019;69(1):7-34.
2. Torre LA, Trabert B, DeSantis CE, Miller KD, Samimi G, Runowicz CD, et al. Ovarian cancer statistics, 2018. CA Cancer J Clin. 2018;68(4):284-96.
3. Andersen CL, Sikora MJ, Boisen MM, Ma T, Christie A, Tseng G, et al. Active Estrogen Receptor-alpha Signaling in Ovarian Cancer Models and Clinical Specimens. Clin Cancer Res. 2017;23(14):3802-12.
4. Meng C, Zhou JQ, Liao YS. Autophagy-related long non-coding RNA signature for ovarian cancer. J Int Med Res. 2020;48(11):300060520970761.
5. Henderson JT, Webber EM, Sawaya GF. Screening for Ovarian Cancer: Updated Evidence Report and Systematic Review for the US Preventive Services Task Force. JAMA. 2018;319(6):595-606.
6. Huang H, Weng H, Chen J. m(6)A Modification in Coding and Non-coding RNAs: Roles and Therapeutic Implications in Cancer. Cancer Cell. 2020;37(3):270-88.
7. Shulman Z, Stern-Ginossar N. The RNA modification N(6)-methyladenosine as a novel regulator of the immune system. Nat Immunol. 2020;21(5):501-12.
8. Roundtree IA, Evans ME, Pan T, He C. Dynamic RNA Modifications in Gene Expression Regulation. Cell. 2017;169(7):1187-200.
9. Wang T, Kong S, Tao M, Ju S. The potential role of RNA N6-methyladenosine in Cancer progression. Mol Cancer. 2020;19(1):88.
10. Bhan A, Soleimani M, Mandal SS. Long Noncoding RNA and Cancer: A New Paradigm. Cancer Res. 2017;77(15):3965-81.
11. Botti G, Scognamiglio G, Aquino G, Liguori G, Cantile M. LncRNA HOTAIR in Tumor Microenvironment: What Role? Int J Mol Sci. 2019;20(9).

12. Peng WX, Koirala P, Mo YY. LncRNA-mediated regulation of cell signaling in cancer. Oncogene. 2017;36(41):5661-7.
13. Chen Y, Lin Y, Shu Y, He J, Gao W. Interaction between N(6)-methyladenosine (m(6)A) modification and noncoding RNAs in cancer. Mol Cancer. 2020;19(1):94.
14. Coker H, Wei G, Brockdorff N. m6A modification of non-coding RNA and the control of mammalian gene expression. Biochim Biophys Acta Gene Regul Mech. 2019;1862(3):310-8.
15. Yi YC, Chen XY, Zhang J, Zhu JS. Novel insights into the interplay between m(6)A modification and noncoding RNAs in cancer. Mol Cancer. 2020;19(1):121.
16. Liu H, Xu Y, Yao B, Sui T, Lai L, Li Z. A novel N6-methyladenosine (m6A)-dependent fate decision for the lncRNA THOR. Cell Death Dis. 2020;11(8):613.
17. Wu Y, Yang X, Chen Z, Tian L, Jiang G, Chen F, et al. m(6)A-induced lncRNA RP11 triggers the dissemination of colorectal cancer cells via upregulation of Zeb1. Mol Cancer. 2019;18(1):87.
18. Dai F, Wu Y, Lu Y, An C, Zheng X, Dai L, et al. Crosstalk between RNA m(6)A Modification and Non-coding RNA Contributes to Cancer Growth and Progression. Mol Ther Nucleic Acids. 2020;22:62-71.
19. Song P, Yang F, Jin H, Wang X. The regulation of protein translation and its implications for cancer. Signal Transduct Target Ther. 2021;6(1):68.
20. Wang Y, Lu JH, Wu QN, Jin Y, Wang DS, Chen YX, et al. LncRNA LINRIS stabilizes IGF2BP2 and promotes the aerobic glycolysis in colorectal cancer. Mol Cancer. 2019;18(1):174.
21. Wang J, Ding W, Xu Y, Tao E, Mo M, Xu W, et al. Long non-coding RNA RHPN1-AS1 promotes tumorigenesis and metastasis of ovarian cancer by acting as a ceRNA against miR-596 and upregulating LETM1. Aging (Albany NY). 2020;12(5):4558-72.
22. Tang Z, Li C, Kang B, Gao G, Li C, Zhang Z. GEPIA: a web server for cancer and normal gene expression profiling and interactive analyses. Nucleic Acids Res. 2017;45(W1):W98-W102.
23. Goldman MJ, Zhang J, Fonseca NA, Cortes-Ciriano I, Xiang Q, Craft B, et al. A user guide for the online exploration and visualization of PCAWG data. Nat Commun. 2020;11(1):3400.
24. Zaccara S, Ries RJ, Jaffrey SR. Reading, writing and erasing mRNA methylation. Nat Rev Mol Cell Biol. 2019;20(10):608-24.
25. Li X, Li Y, Yu X, Jin F. Identification and validation of stemness-related lncRNA prognostic signature for breast cancer. J Transl Med. 2020;18(1):331.
26. Liu J, Xu W, Li S, Sun R, Cheng W. Multi-omics analysis of tumor mutational burden combined with prognostic assessment in epithelial ovarian cancer based on TCGA database. Int J Med Sci. 2020;17(18):3200-13.
27. Yu G, Wang LG, Han Y, He QY. clusterProfiler: an R package for comparing biological themes among gene clusters. OMICS. 2012;16(5):284-7.
28. Newman AM, Liu CL, Green MR, Gentles AJ, Feng W, Xu Y, et al. Robust enumeration of cell subsets from tissue expression profiles. Nat Methods. 2015;12(5):453-7.

29. Yoshihara K, Shahmoradgoli M, Martinez E, Vegesna R, Kim H, Torres-Garcia W, et al. Inferring tumour purity and stromal and immune cell admixture from expression data. Nat Commun. 2013;4:2612.
30. Charoentong P, Finotello F, Angelova M, Mayer C, Efremova M, Rieder D, et al. Pan-cancer Immunogenomic Analyses Reveal Genotype-Immunophenotype Relationships and Predictors of Response to Checkpoint Blockade. Cell Rep. 2017;18(1):248-62.
31. Reinhold WC, Sunshine M, Varma S, Doroshow JH, Pommier Y. Using CellMiner 1.6 for Systems Pharmacology and Genomic Analysis of the NCI-60. Clin Cancer Res. 2015;21(17):3841-52.
32. Thorsson V, Gibbs DL, Brown SD, Wolf D, Bortone DS, Ou Yang TH, et al. The Immune Landscape of Cancer. Immunity. 2018;48(4):812-30 e14.
33. Webb PM, Jordan SJ. Epidemiology of epithelial ovarian cancer. Best Pract Res Clin Obstet Gynaecol. 2017;41:3-14.
34. Shen S, Wang G, Zhang R, Zhao Y, Yu H, Wei Y, et al. Development and validation of an immune gene-set based Prognostic signature in ovarian cancer. EBioMedicine. 2019;40:318-26.
35. Millstein J, Budden T, Goode EL, Anglesio MS, Talhouk A, Intermaggio MP, et al. Prognostic gene expression signature for high-grade serous ovarian cancer. Ann Oncol. 2020;31(9):1240-50.
36. Liu J, Meng H, Nie S, Sun Y, Jiang P, Li S, et al. Identification of a prognostic signature of epithelial ovarian cancer based on tumor immune microenvironment exploration. Genomics. 2020;112(6):4827-41.
37. Zheng M, Hu Y, Gou R, Nie X, Li X, Liu J, et al. Identification three LncRNA prognostic signature of ovarian cancer based on genome-wide copy number variation. Biomed Pharmacother. 2020;124:109810.
38. Fan L, Lin Y, Lei H, Shu G, He L, Yan Z, et al. A newly defined risk signature, consisting of three m(6)A RNA methylation regulators, predicts the prognosis of ovarian cancer. Aging (Albany NY). 2020;12(18):18453-75.
39. Han D, Liu J, Chen C, Dong L, Liu Y, Chang R, et al. Anti-tumour immunity controlled through mRNA m(6)A methylation and YTHDF1 in dendritic cells. Nature. 2019;566(7743):270-4.
40. Wang H, Hu X, Huang M, Liu J, Gu Y, Ma L, et al. Mettl3-mediated mRNA m(6)A methylation promotes dendritic cell activation. Nat Commun. 2019;10(1):1898.
41. Wang Q, Chen C, Ding Q, Zhao Y, Wang Z, Chen J, et al. METTL3-mediated m(6)A modification of HDGF mRNA promotes gastric cancer progression and has prognostic significance. Gut. 2020;69(7):1193-205.
42. Zhang B, Wu Q, Li B, Wang D, Wang L, Zhou YL. m(6)A regulator-mediated methylation modification patterns and tumor microenvironment infiltration characterization in gastric cancer. Mol Cancer. 2020;19(1):53.
43. Lan Q, Liu PY, Haase J, Bell JL, Huttelmaier S, Liu T. The Critical Role of RNA m(6)A Methylation in Cancer. Cancer Res. 2019;79(7):1285-92.

44. He L, He G. DNM3OS Facilitates Ovarian Cancer Progression by Regulating miR-193a-3p/MAP3K3 Axis. Yonsei Med J. 2021;62(6):535-44.
45. Xia X, Zhang H, Xia P, Zhu Y, Liu J, Xu K, et al. Identification of Glycolysis-Related lncRNAs and the Novel lncRNA WAC-AS1 Promotes Glycolysis and Tumor Progression in Hepatocellular Carcinoma. Front Oncol. 2021;11:733595.
46. Zheng J, Zhou Z, Qiu Y, Wang M, Yu H, Wu Z, et al. A Prognostic Ferroptosis-Related lncRNAs Signature Associated With Immune Landscape and Radiotherapy Response in Glioma. Front Cell Dev Biol. 2021;9:675555.
47. Shi Z, Shen C, Yu C, Yang X, Shao J, Guo J, et al. Long non-coding RNA LINC00997 silencing inhibits the progression and metastasis of colorectal cancer by sponging miR-512-3p. Bioengineered. 2021;12(1):627-39.
48. Odunsi K. Immunotherapy in ovarian cancer. Ann Oncol. 2017;28(suppl_8):viii1-viii7.
49. Hartnett EG, Knight J, Radolec M, Buckanovich RJ, Edwards RP, Vlad AM. Immunotherapy Advances for Epithelial Ovarian Cancer. Cancers (Basel). 2020;12(12).
50. Ovarian Tumor Tissue Analysis C, Goode EL, Block MS, Kalli KR, Vierkant RA, Chen W, et al. Dose-Response Association of CD8+ Tumor-Infiltrating Lymphocytes and Survival Time in High-Grade Serous Ovarian Cancer. JAMA Oncol. 2017;3(12):e173290.
51. Tamborero D, Rubio-Perez C, Muinos F, Sabarinathan R, Piulats JM, Muntasell A, et al. A Pan-cancer Landscape of Interactions between Solid Tumors and Infiltrating Immune Cell Populations. Clin Cancer Res. 2018;24(15):3717-28.
52. Kreuzinger C, Geroldinger A, Smeets D, Braicu EI, Sehouli J, Koller J, et al. A Complex Network of Tumor Microenvironment in Human High-Grade Serous Ovarian Cancer. Clin Cancer Res. 2017;23(24):7621-32.
53. Zheng J, Guo J, Cao B, Zhou Y, Tong J. Identification and validation of lncRNAs involved in m6A regulation for patients with ovarian cancer. Cancer Cell Int. 2021;21(1):363.
54. Wei Q, Yang D, Liu X, Zhao H, Yang Y, Xu J, et al. Exploration of the Role of m(6) A RNA Methylation Regulators in Malignant Progression and Clinical Prognosis of Ovarian Cancer. Front Genet. 2021;12:650554.
55. Olbrecht S, Busschaert P, Qian J, Vanderstichele A, Loverix L, Van Gorp T, et al. High-grade serous tubo-ovarian cancer refined with single-cell RNA sequencing: specific cell subtypes influence survival and determine molecular subtype classification. Genome Med. 2021;13(1):111.
56. Tan Q, Liu H, Xu J, Mo Y, Dai F. Integrated analysis of tumor-associated macrophage infiltration and prognosis in ovarian cancer. Aging (Albany NY). 2021;13(19):23210-32.
57. Gao Y, Xu Y, Zhao S, Qian L, Song T, Zheng J, et al. Growth differentiation factor-15 promotes immune escape of ovarian cancer via targeting CD44 in dendritic cells. Exp Cell Res. 2021;402(1):112522.
58. Zhu H, Blum RH, Bjordahl R, Gaidarova S, Rogers P, Lee TT, et al. Pluripotent stem cell-derived NK cells with high-affinity noncleavable CD16a mediate improved antitumor activity. Blood.

2020;135(6):399-410.
59. Klingemann H, Boissel L, Toneguzzo F. Natural Killer Cells for Immunotherapy - Advantages of the NK-92 Cell Line over Blood NK Cells. Front Immunol. 2016;7:91.
60. Motz GT, Coukos G. Deciphering and reversing tumor immune suppression. Immunity. 2013;39(1):61-73.
61. Banchereau R, Leng N, Zill O, Sokol E, Liu G, Pavlick D, et al. Molecular determinants of response to PD-L1 blockade across tumor types. Nat Commun. 2021;12(1):3969.
62. Maiorano BA, Maiorano MFP, Lorusso D, Maiello E. Ovarian Cancer in the Era of Immune Checkpoint Inhibitors: State of the Art and Future Perspectives. Cancers (Basel). 2021;13(17).
63. Yang C, Xia BR, Zhang ZC, Zhang YJ, Lou G, Jin WL. Immunotherapy for Ovarian Cancer: Adjuvant, Combination, and Neoadjuvant. Front Immunol. 2020;11:577869.
64. Miao YR, Thakkar KN, Qian J, Kariolis MS, Huang W, Nandagopal S, et al. Neutralization of PD-L2 is Essential for Overcoming Immune Checkpoint Blockade Resistance in Ovarian Cancer. Clin Cancer Res. 2021;27(15):4435-48.
65. Liu YT, Sun ZJ. Turning cold tumors into hot tumors by improving T-cell infiltration. Theranostics. 2021;11(11):5365-86.
66. Chen DS, Mellman I. Elements of cancer immunity and the cancer-immune set point. Nature. 2017;541(7637):321-30.
67. Bruni D, Angell HK, Galon J. The immune contexture and Immunoscore in cancer prognosis and therapeutic efficacy. Nat Rev Cancer. 2020;20(11):662-80.
68. Hegde PS, Karanikas V, Evers S. The Where, the When, and the How of Immune Monitoring for Cancer Immunotherapies in the Era of Checkpoint Inhibition. Clin Cancer Res. 2016;22(8):1865-74.
69. Gu J, Bi F. Significance of N6-Methyladenosine RNA Methylation Regulators in Immune Infiltrates of Ovarian Cancer. Front Genet. 2021;12:671179.
70. Jiang Y, Wan Y, Gong M, Zhou S, Qiu J, Cheng W. RNA demethylase ALKBH5 promotes ovarian carcinogenesis in a simulated tumour microenvironment through stimulating NF-kappaB pathway. J Cell Mol Med. 2020;24(11):6137-48.
71. Das S, Reddy MA, Senapati P, Stapleton K, Lanting L, Wang M, et al. Diabetes Mellitus-Induced Long Noncoding RNA Dnm3os Regulates Macrophage Functions and Inflammation via Nuclear Mechanisms. Arterioscler Thromb Vasc Biol. 2018;38(8):1806-20.
72. Lakhia R, Yheskel M, Flaten A, Ramalingam H, Aboudehen K, Ferre S, et al. Interstitial microRNA miR-214 attenuates inflammation and polycystic kidney disease progression. JCI Insight. 2020;5(7).

Figures

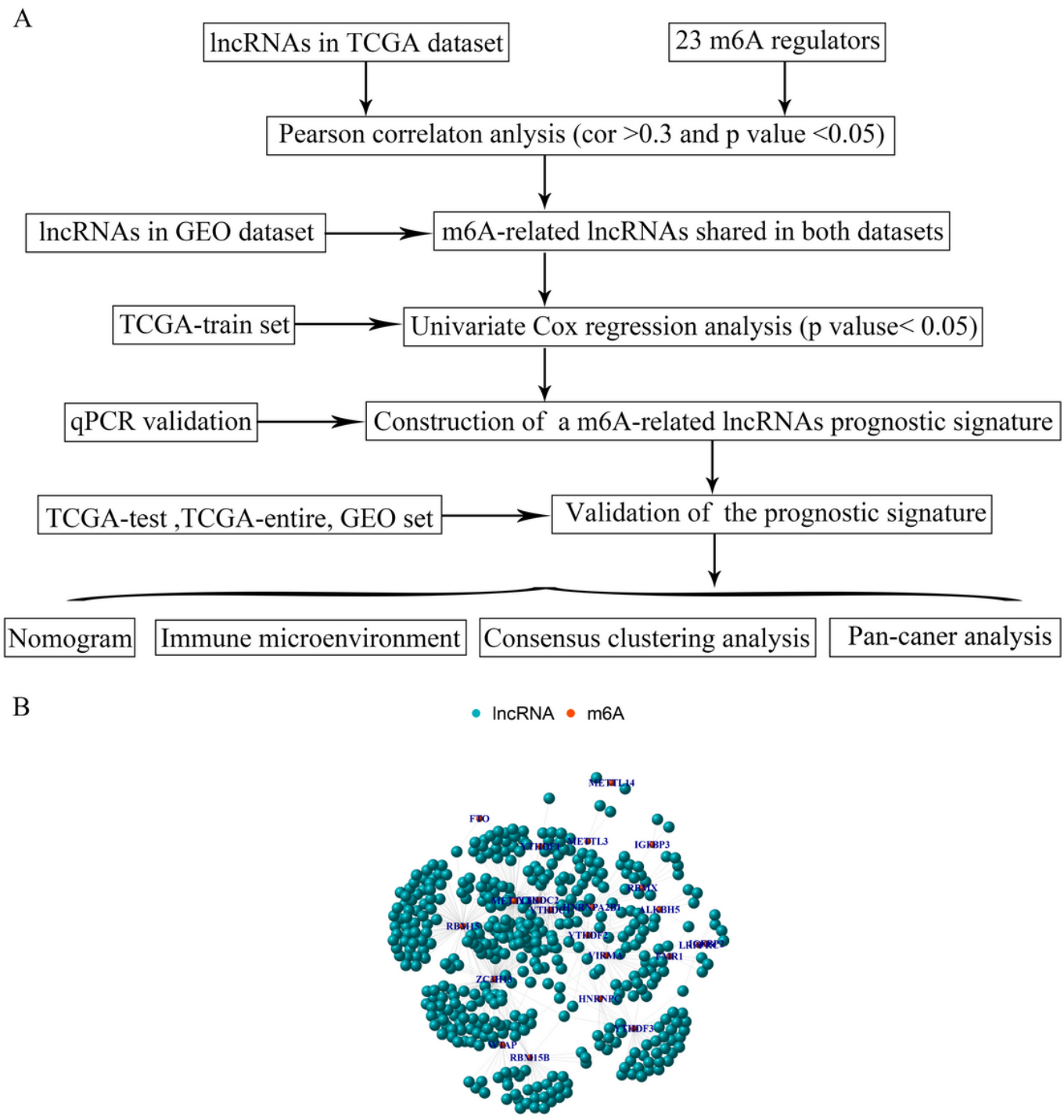

Figure 1

(A) Flow chart of the study and (B) Co-expression network diagram of m6A regulators and lncRNAs in TCGA dataset.

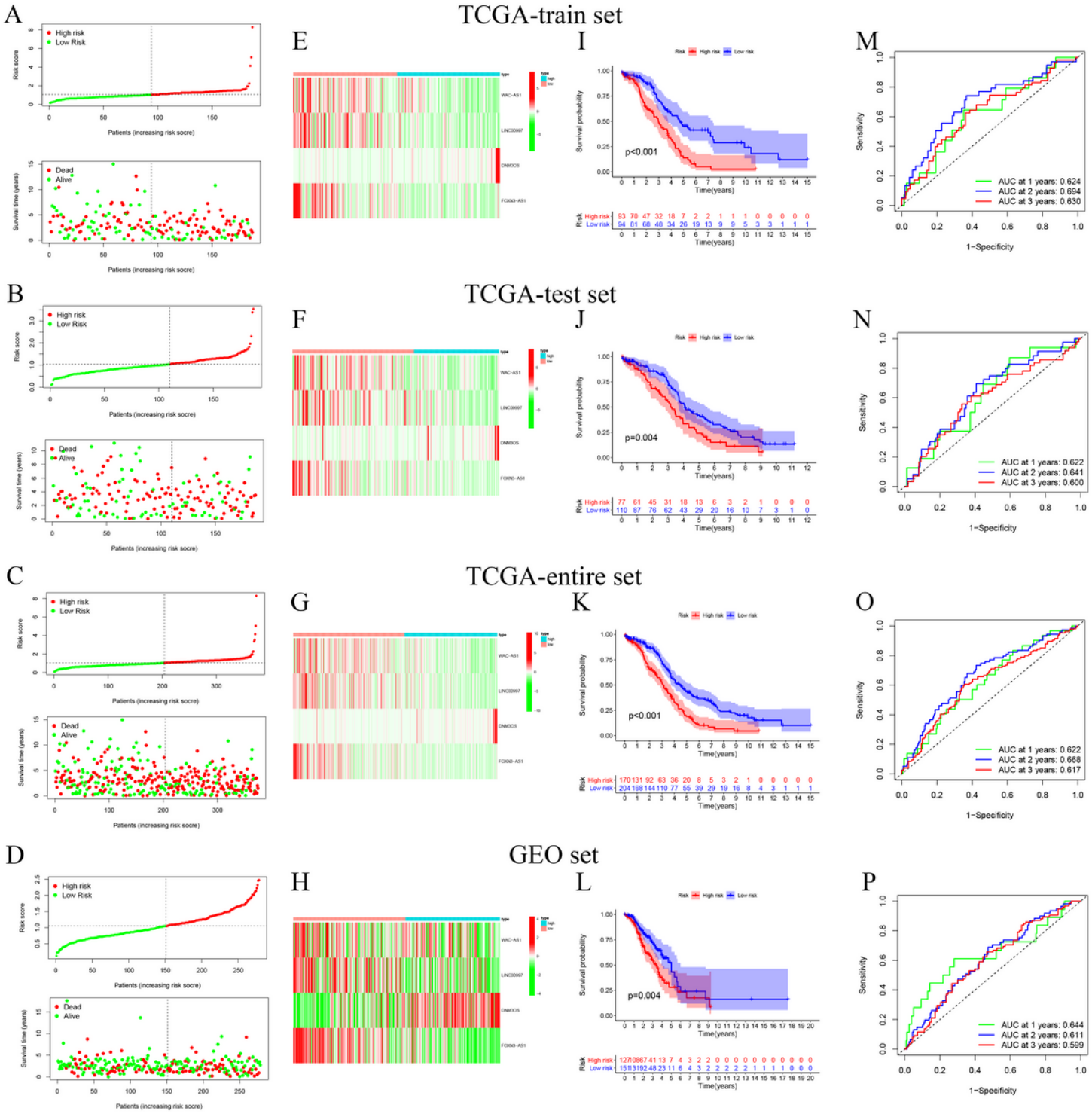

Figure 2

Construction and Validation of the mRLs prognostic signature. Distribution of risk score, OS status (A-D) and heatmap of the expression of the four prognostic mRLs (E-H) in the TCGA-train, test, entire and GEO dataset. (I-L) Kaplan-Meier curves of OS for OV patients with high or low risk score in the TCGA-train, test, entire and GEO dataset. (M-P) Time-dependent ROC analysis of risk score in predicting prognoses in the TCGA-train, test, entire and GEO dataset. ROC, receiver operating characteristic. In TCGA-train set, N=187; in TCGA-test set, N=187; in TCGA-entire set, N=374; in GEO set, N=278.

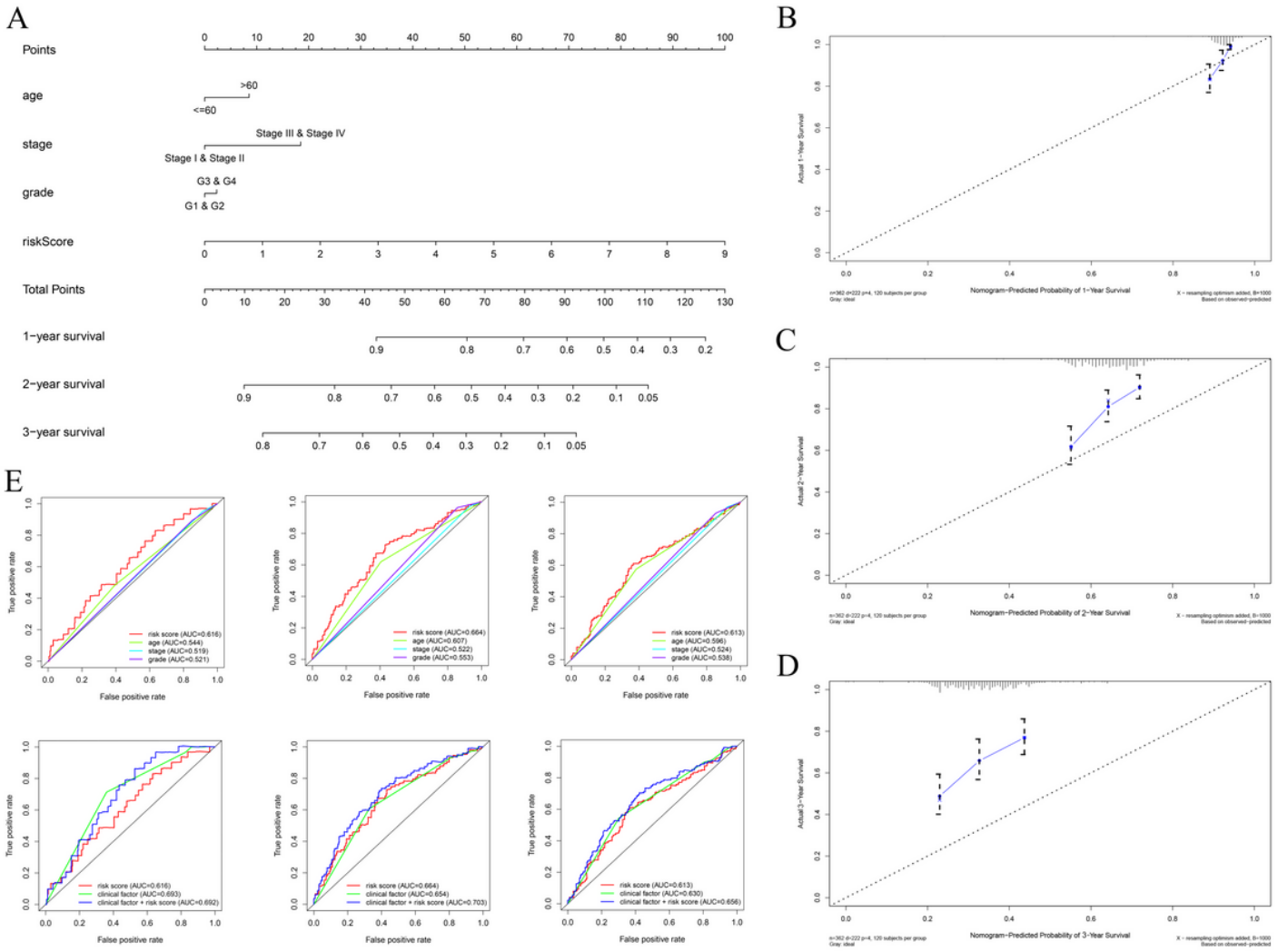

Figure 3

A nomogram for OV patients in TCGA dataset. (A) A nomogram for predicting the 1-, 2-, and 3-year OS of OV patients. (B-D) Calibration curves for the prediction of 1-, 2- or 3-year overall survival of OV patients. (E) Time-dependent ROC curves for each parameter and the combination of independent prognostic risk factors in the TCGA dataset (for predicting 1, 2, and 3-year OS).In TCGA-entire set, N=374.

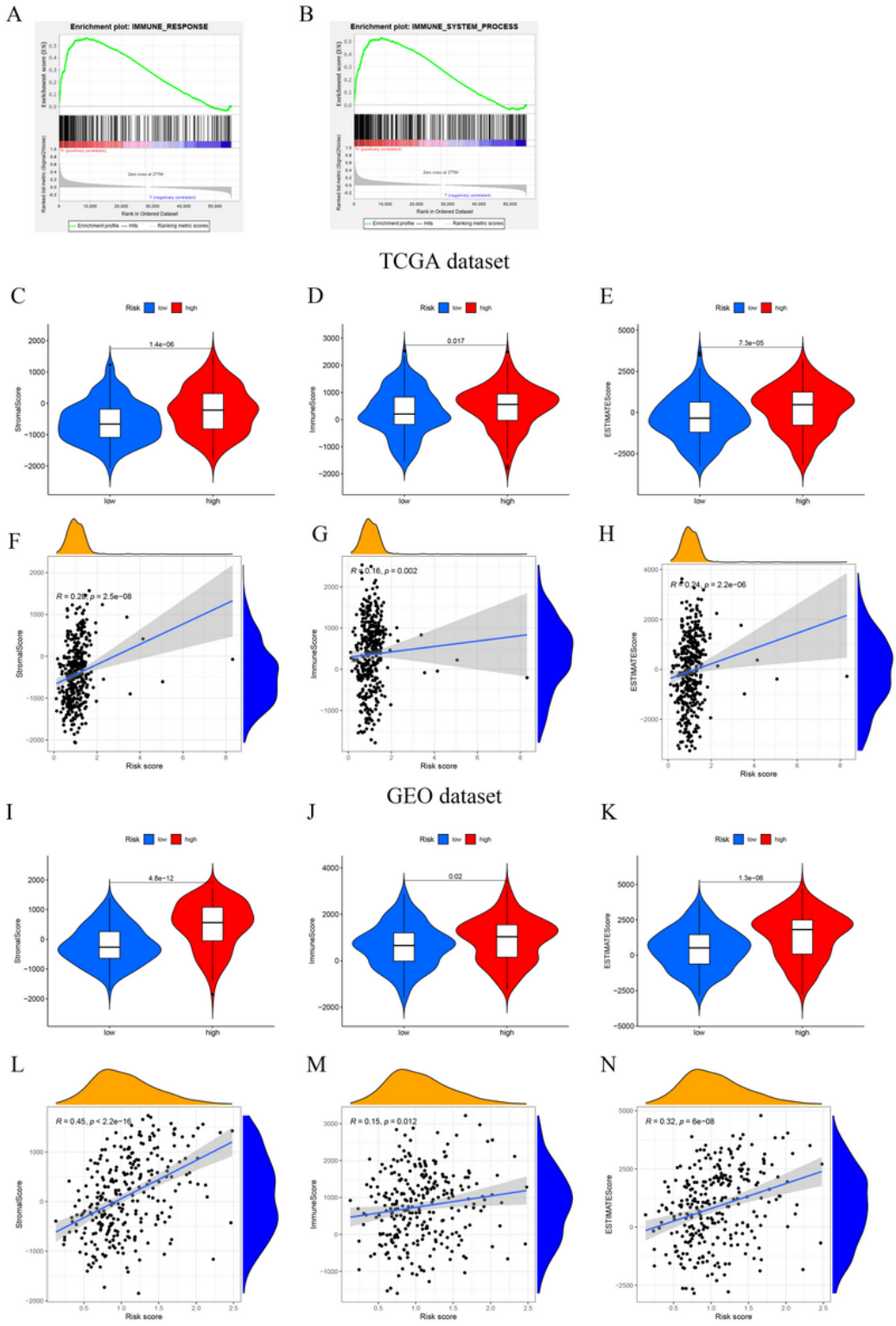

Figure 4

The correlation between risk score and immune features in the TCGA dataset. (A-B) GSEA showed that immune response and immune system process were enriched in high-risk group. (C-E) Stroma, immune, and ESTIMATE scores in the high- and low-risk groups in TCGA dataset. (F-H) The correlation between risk score and Stroma, immune, and ESTIMATE scores in TCGA dataset. (I-K) Stroma, immune, and ESTIMATE scores in the high- and low-risk groups in GEO dataset. (L-N) The correlation between risk

score and Stroma, immune, and ESTIMATE scores in GEO dataset. In TCGA-entire set, N=374; in GEO set, N=278.

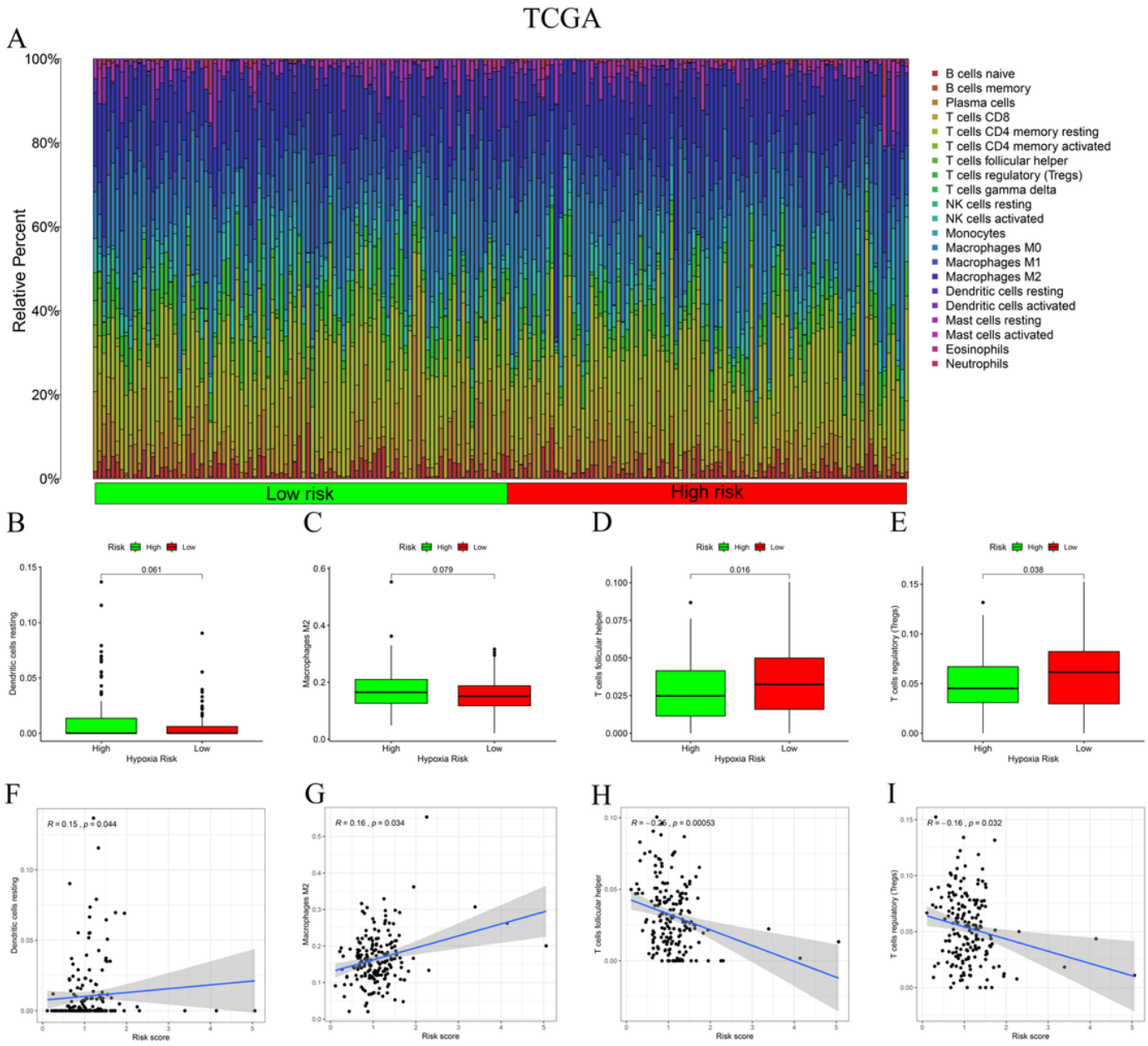

Figure 5

Relationships between the risk score and immune cell infiltration and the role of the mRLs in tumor microenvironment in TCGA dataset. (A) The proportion of 22 immune cells infiltration in high- and low-risk groups. (B-I) Correlation of expression of the mRLs and infiltration of specific immune cell type. Iin TCGA-entire set, N=374.

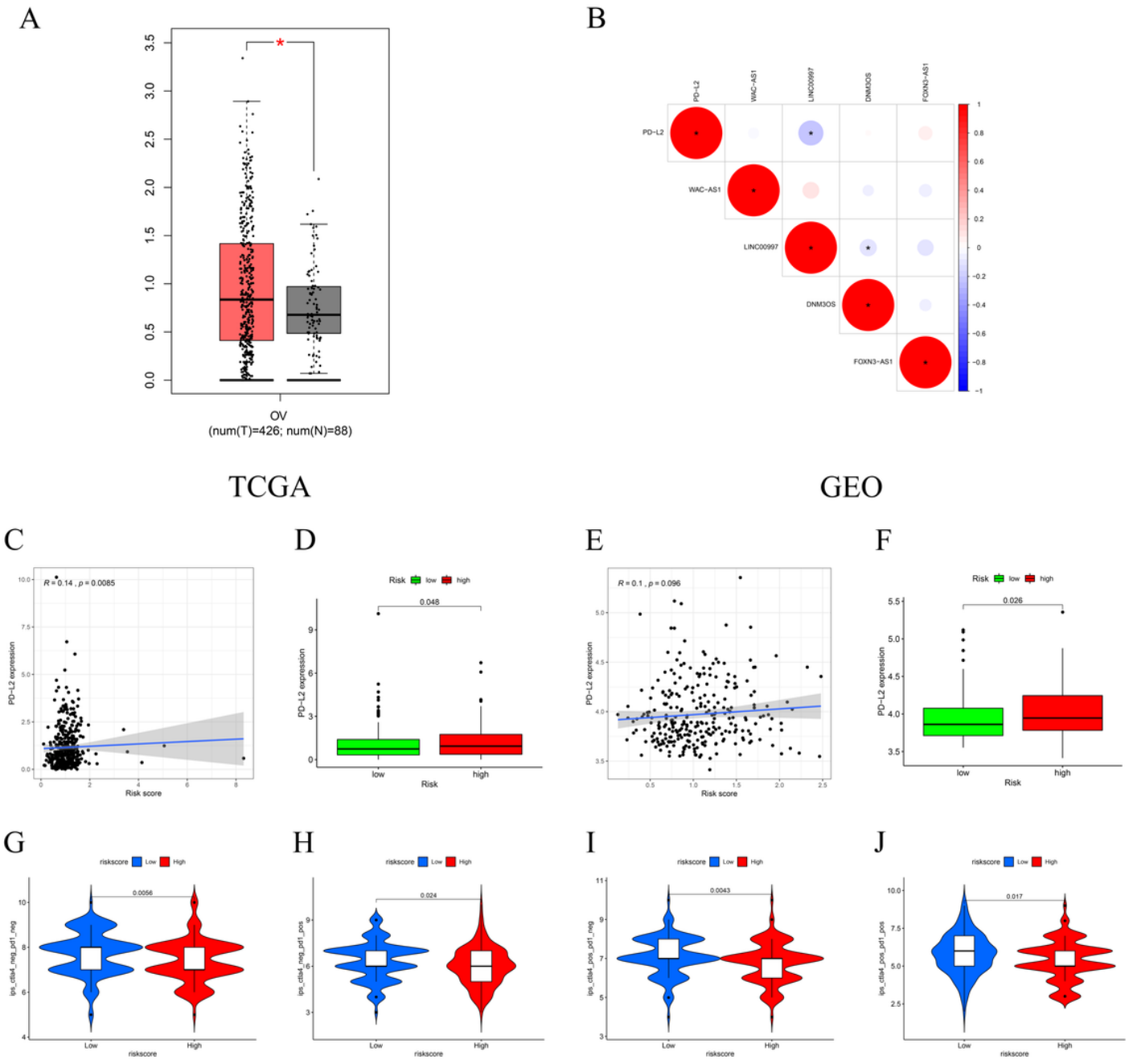

Figure 6

IPSs and immunotherapy gene expression analysis. (A) The expression of PD-L2 in tumor and normal tissues. (B) The correlation between the mRLs and PD-L2. (C-F) The expression of PD-L2 in low- and high-risk groups in TCGA and GEO datasets. (G-J) The IPSs of low- and high- risk groups. *P < 0.05, **P < 0.01, and ***P < 0.001. In TCGA-entire set, N=374; in GEO set, N=278.

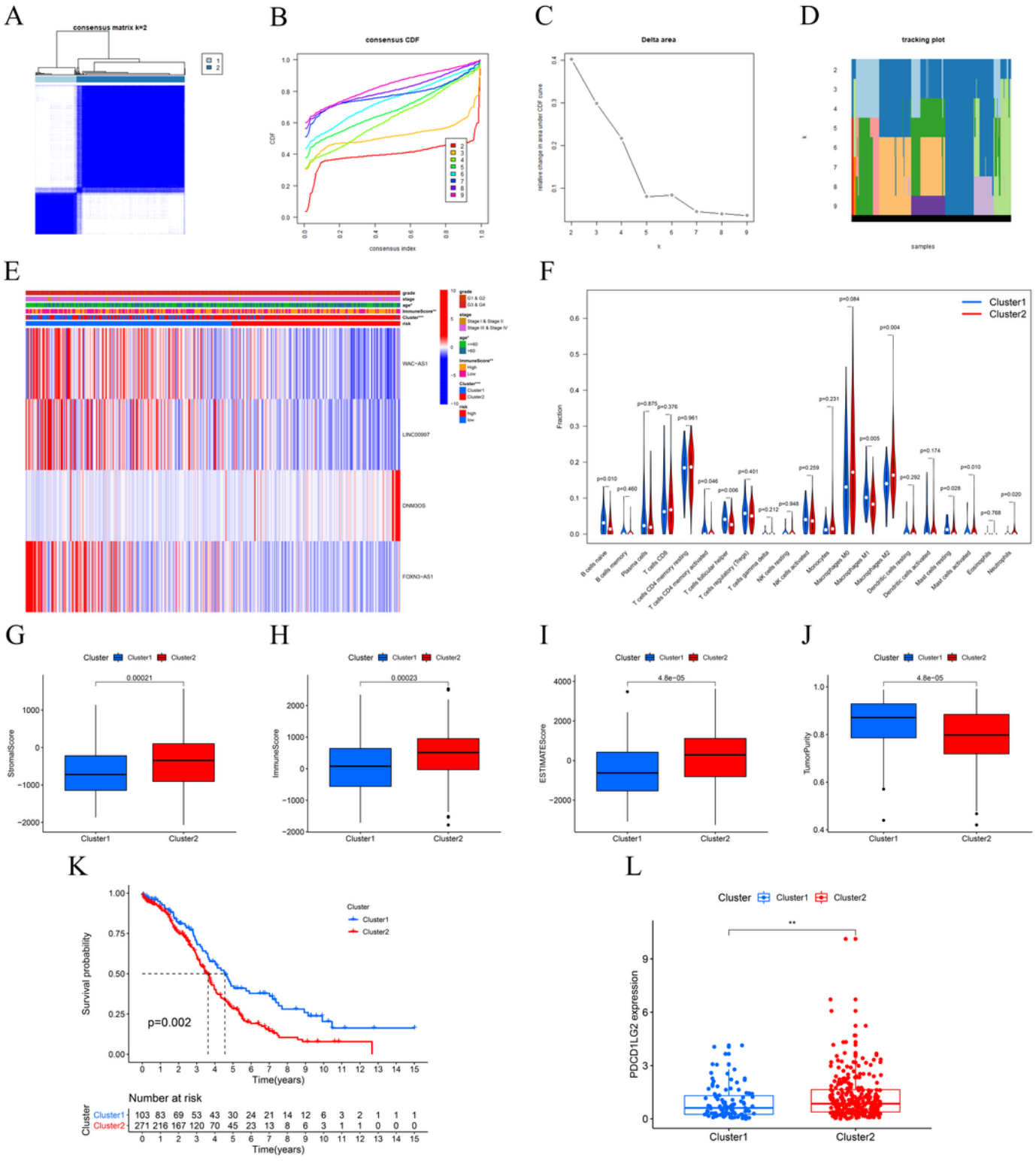

Figure 7

Prognosis and immune infiltrations in consensus clustering subgroups of OV. (A) Consensus clustering matrix for k = 2. (B) Consensus clustering cumulative distribution function (CDF) for k=2 to 9. (C) Relative change in area under the CDF curve for k=2 to 9. (D) Tracking plot for k=2 to 9. (E) Expression pattern of the mRLs in Cluster1 and Cluster2 subgroups. (F) The abundance of 21 immune cells in Cluster1 and Cluster2 subgroups. (G-J) Stroma, immune, and ESTIMATE scores and tumor purity in Cluster1 and

Cluster2 subgroups. (K) Kaplan–Meier analysis of patients in Cluster1 and Cluster2 subgroups. (L) The expression of PD-L2 in in Cluster1 and Cluster2 subgroups.

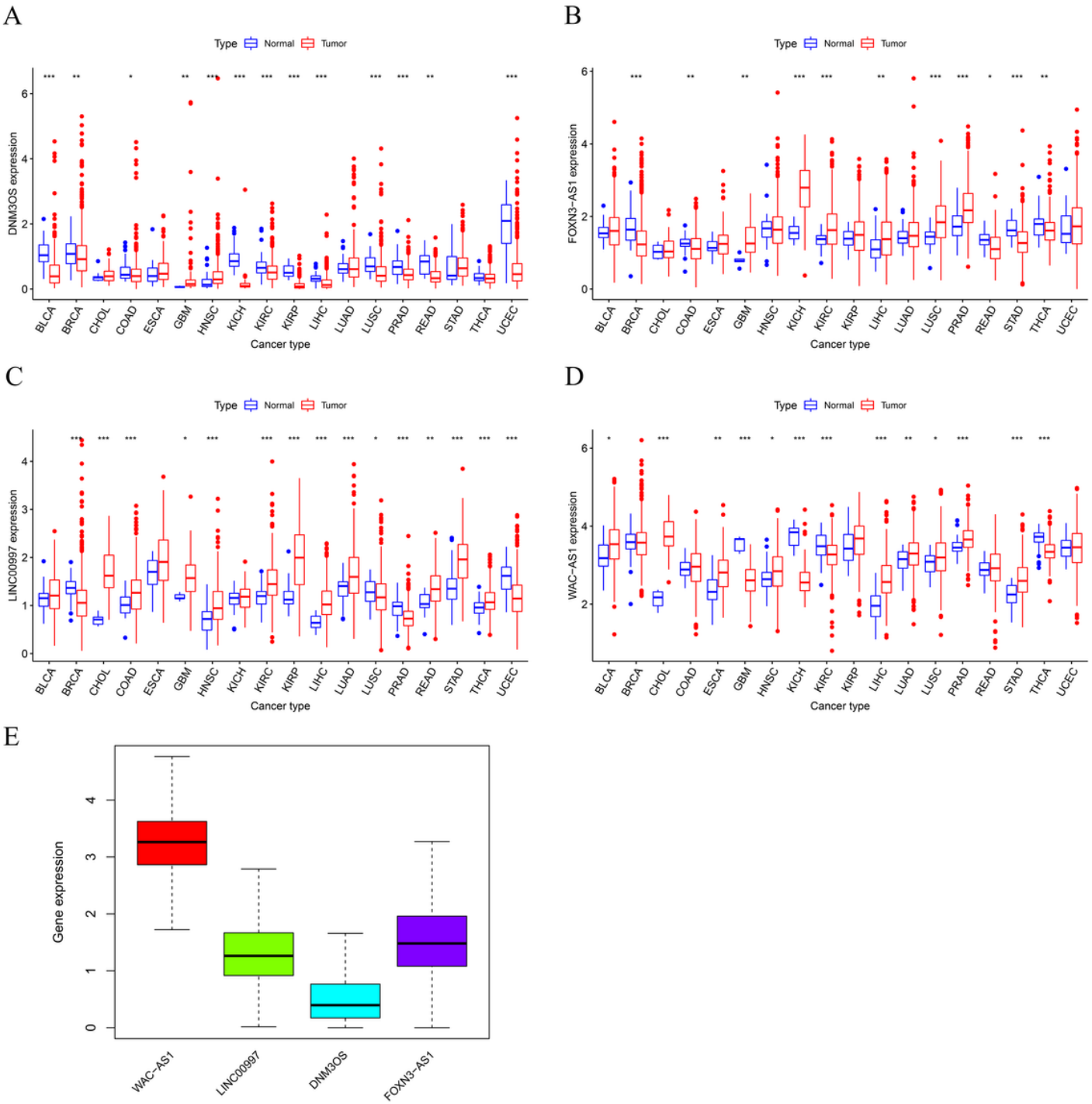

Figure 8

Expression of pan-cancer the mRLs. (A-D) Boxplot showing the expression level of the mRLs in tumor tissue compared with normal tissue in 18 cancer types which were composed of at least 5 normal samples. (E) Boxplot showing the expression distribution of the mRLs across pan-cancer.

Figure 9

Association of expression of the mRLs with immune subtypes, tumor microenvironment and cancer stemness in pan-cancer. (A)Association of expression of the m6A-related lncRNA with immune infiltrate subtypes across all the cancer types tested with ANOVA. (B-C) Correlation matrix between tumor microenvironment stromal scores (B) and immune scores (C) and the mRLs expression by ESTIMATE algorithm. (D-E) Correlation matrix plots showing the association between the m6A-related genes expression and cancer stemness DNAss score (D), and RNAss score (E).

Supplementary Files

This is a list of supplementary files associated with this preprint. Click to download.

- FigureS1.tif
- FigureS2.tif
- FigureS3.tif
- FigureS4.tif
- FigureS5.tif
- FigureS6.tif
- FigureS7.tif
- FigureS8.tif
- FigureS9.tif
- FigureS10.tif
- TableS1.docx